The Journal of Immunology

Antigen Recognition in the Islets Changes with Progression of Autoimmune Islet Infiltration

Robin S. Lindsay, Kaitlin Corbin, Ashley Mahne, Bonnie E. Levitt, Matthew J. Gebert, Eric J. Wigton, Brenda J. Bradley, Kathryn Haskins, Jordan Jacobelli, Qizhi Tang, Matthew F. Krummel and Rachel S. Friedman

J Immunol 2015; 194:522-530; Prepublished online 10 December 2014;
doi: 10.4049/jimmunol.1400626
http://www.jimmunol.org/content/194/2/522

The Journal of Immunology is published twice each month by
The American Association of Immunologists, Inc.,
9650 Rockville Pike, Bethesda, MD 20814-3994.

Print ISSN: 0022-1767 Online ISSN: 1550-6606.

Antigen Recognition in the Islets Changes with Progression of Autoimmune Islet Infiltration

Robin S. Lindsay,*,† Kaitlin Corbin,‡ Ashley Mahne,§ Bonnie E. Levitt,* Matthew J. Gebert,* Eric J. Wigton,* Brenda J. Bradley,*,† Kathryn Haskins,*,† Jordan Jacobelli,*,† Qizhi Tang,§ Matthew F. Krummel,‡ and Rachel S. Friedman*,†

In type 1 diabetes, the pancreatic islets are an important site for therapeutic intervention because immune infiltration of the islets is well established at diagnosis. Therefore, understanding the events that underlie the continued progression of the autoimmune response and islet destruction is critical. Islet infiltration and destruction is an asynchronous process, making it important to analyze the disease process on a single islet basis. To understand how T cell stimulation evolves through the process of islet infiltration, we analyzed the dynamics of T cell movement and interactions within individual islets of spontaneously autoimmune NOD mice. Using both intravital and explanted two-photon islet imaging, we defined a correlation between increased islet infiltration and increased T cell motility. Early T cell arrest was Ag dependent and due, at least in part, to Ag recognition through sustained interactions with CD11c$^+$ APCs. As islet infiltration progressed, T cell motility became Ag independent, with a loss of T cell arrest and sustained interactions with CD11c$^+$ APCs. These studies suggest that the autoimmune T cell response in the islets may be temporarily dampened during the course of islet infiltration and disease progression. ***The Journal of Immunology*****, 2015, 194: 522–530.**

Type 1 diabetes (T1D) results from the autoimmune destruction of pancreatic β cells, primarily by autoreactive T cells. As the site of pathogenesis, the islets are the location for maintenance of the autoimmune response once infiltration begins (1). With current diagnostic methods, treatments must be effective following disease establishment, making the islets a critical site for therapeutic intervention. Importantly, islet infiltration by immune cells is an asynchronous process, meaning that an individual pancreas can contain islet infiltration states that vary from untouched to destroyed (2). Pooled islet analyses average this heterogeneity, potentially missing important information about key stages of the autoimmune process. Live imaging allows for the determination of cellular behaviors at distinct stages of the autoimmune response, permitting analysis of the immune response on an islet-by-islet basis.

The NOD mouse is regarded as the mouse model of T1D that best replicates the human disease (3). By 4 wk of age in the NOD mouse, T cells infiltrate the pancreatic islets (4), and the pancreatic lymph nodes are no longer required for disease progression (1). Like in the human disease, islet destruction in the NOD mouse proceeds in an asynchronous manner (3). T cells can organize into peri-insulitic infiltrates (4) or tertiary lymphoid structures (5) prior to islet destruction. Whereas the mechanism remains unclear, mice that are resistant to diabetes can have islet infiltration and peri-insulitis that does not progress to diabetes (6). It is likely that peripheral tolerance mechanisms, including regulatory T cells (Tregs) (7, 8), restrain the T cell–mediated destruction of the β cells during peri-insulitis. The islets are also a site of T cell stimulation, demonstrated by induction of autoreactive T cell effector function (9), and development of effector memory cells (10). However, little is known about the series of events leading to the stimulation of T cells within the islets.

Intravital and explanted imaging of islets have been used in diabetes and islet transplant models. Imaging of explanted islets has been used to quantify APC infiltration of islets (11) and identify APC–T cell interactions within the islets (9, 12). Intravital islet imaging has been used to demonstrate the distinct morphology of the islet vasculature and analyze blood flow rate within the islets (13). Using a transplant model in the anterior chamber of the eye, toxin-induced β cell death (14), the dynamics of T cell–mediated graft rejection (15), and autoimmune attack of islet transplants (16) have been analyzed. A virally induced diabetes model was used to examine the autoimmune response within the pancreas through analysis of CD8 T cell motility and interactions with β cells (17). This study showed direct CD8 T cell–mediated killing of β cells.

Analysis of T cell motility and interactions within the lymph node has established that increased T cell motility and aborted T cell interactions with APCs are associated with tolerance induction, whereas increased duration of T cell arrest and sustained interactions with APCs result in T cell activation (18–21). Multiple mechanisms leading to this effect have been demonstrated in the pancreatic lymph nodes of NOD mice. Motility of Th cells increased within Ag-bearing NOD pancreatic lymph nodes in the presence of Tregs, demonstrating that Treg-induced tolerance

*Department of Biomedical Research, National Jewish Health, Denver, CO 80206; †Department of Immunology and Microbiology, University of Colorado School of Medicine, Denver, CO 80206; ‡Department of Pathology, University of California San Francisco, San Francisco, CA 94143; and §Department of Surgery, University of California San Francisco, San Francisco, CA 94143

Received for publication March 11, 2014. Accepted for publication November 4, 2014.

This work was supported by JDRF Grant 2-2012-197 (to R.S.F.), JDRF Grant 5-2013-200 (to R.S.F. and J.J.), National Jewish Health (to R.S.F. and J.J.), Cancer Research Institute Grant 63003254 (to R.S.L.), JDRF Grant 2007-170 (to M.F.K.), National Institutes of Health Grants R01 DK08231 (to Q.T.) and P30 DK063720 (to Q.T.), and the Sandler Family Foundation (to M.F.K.).

Address correspondence and reprint requests to Dr. Rachel S. Friedman, Department of Biomedical Research, National Jewish Health; Department of Immunology and Microbiology, University of Colorado, 1400 Jackson Street, K501, Denver, CO 80206. E-mail address: FriedmanR@NJHealth.org

The online version of this article contains supplemental material.

Abbreviations used in this article: MSD, mean squared displacement; RIP, rat insulin promoter; T1D, type 1 diabetes; Treg, regulatory T cell; WT, wild-type.

www.jimmunol.org/cgi/doi/10.4049/jimmunol.1400626

mechanisms are associated with increased T cell motility (7). Also, in the NOD model, tolerance induced by transfer of Ag-pulsed, fixed APCs was broken by PD-L1 blockade. This break in tolerance resulted in T cell arrest in both the pancreatic lymph nodes and transplanted islets (22). Both of these studies also demonstrated that the T cell arrest in the lymph nodes was associated with increased T cell–APC interactions (7, 22). These established patterns of T cell motility within lymphoid tissue provide a baseline for understanding the significance of T cell motility changes within the islets during autoimmune attack.

We recently analyzed CD8 T cell motility and interactions with $CD11c^+$ APCs in the pancreatic islets using a model in which islet infiltration was induced by transfer of OT-I T cells into rat insulin promoter (RIP)–mOva B6 mice (9). This study demonstrated that, in the islets, CD8 T cell motility increased, interactions with $CD11c^+$ APCs decreased, and effector cytokine production decreased with progression of islet infiltration (9). However, overt diabetes occurred in only a minority of animals. Deletional tolerance prevents ongoing autoimmunity in the remaining animals, making it unclear whether changes in T cell motility and interactions were reflective of the re-establishment of tolerance. Additionally, because the study used very high-affinity neo-Ag–specific T cells, it was unclear whether the same behavior would occur using islet-Ag–specific T cells in a spontaneous model of T1D. Finally, the study concluded that environmental changes caused the change in T cell behavior, but did not identify what those environmental factors were.

To further examine T cell motility and interactions with APCs within the pancreatic islets of spontaneously autoimmune NOD model of diabetes and determine the requirement for Ag, we used and validated two methods of live islet imaging by two-photon microscopy. These techniques revealed changes in CD4 effector T cell behavior as islet infiltration progressed in the NOD model, which paralleled those observed in OT-I CD8 T cells in the RIP-mOva model, including increased T cell motility and reduced T cell arrest. In this study, we further examined the role of Ag in these changes in T cell motility and interactions. In the absence of specific Ag in the islets, T cell motility was increased early in the progression of islet infiltration, suggesting that the arrest observed was a result of Ag presentation and recognition. However, the dependence on Ag was reduced as infiltration progressed. Additionally, as islet infiltration progressed, T cell–$CD11c^+$ APC contacts were decreased in duration, but not in frequency. These data support the hypothesis that T cell arrest in early stages of islet infiltration is due to T cell interactions with Ag-bearing APCs within the islets, but, as islet infiltration increases, environmental factors override Ag recognition, leading to a loss of T cell–APC interactions within the islet.

Materials and Methods

Mice

NOD/ShiLtJ (Jackson 001976), C57BL/6.MIP-GFP (Jackson 006864), and NOD.CD11c-YFP (Jackson 009422) (23) mice were obtained from The Jackson Laboratory; NOD.BDC-2.5 TCR transgenic (24), NOD.BDC-6.9 TCR transgenic (25), and NOD.C6 (25) were bred in house by the Haskins laboratory. All animal procedures were approved by the Institutional Animal Care and Use Committee committees at National Jewish Health and University of California San Francisco.

Intravital surgery

Anesthesia was induced with ketamine (50 μg/g) (Vedco)/xylazine (5 μg/g) (JHP) by i.p. injection and maintained using inhaled isoflourane (2–3% in

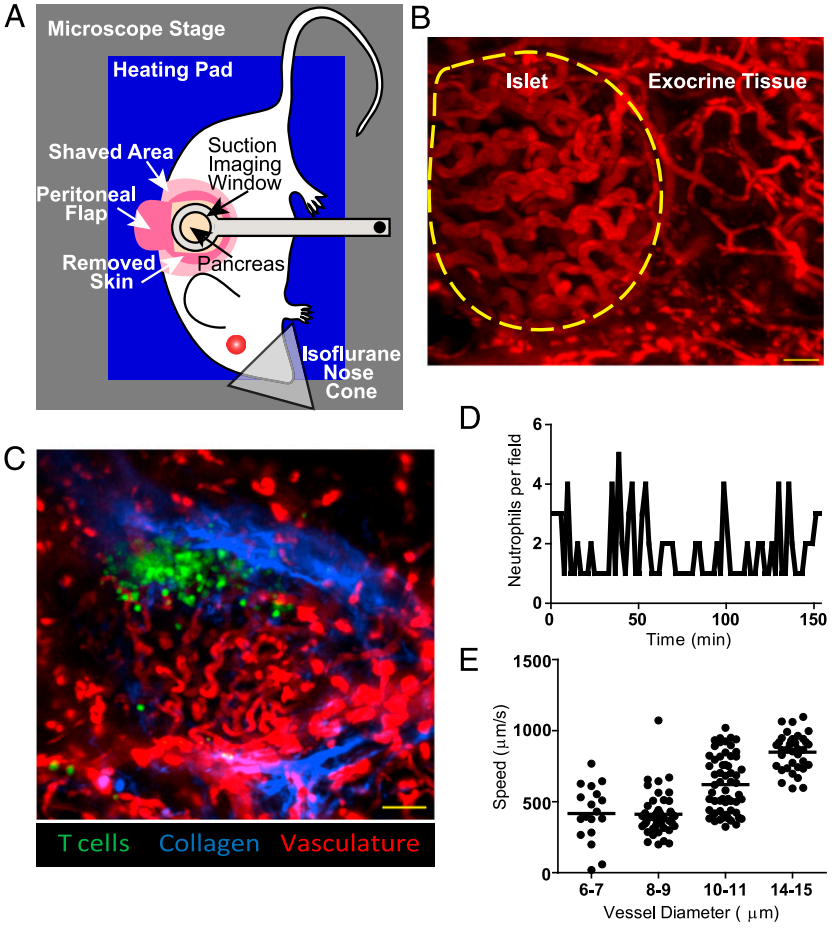

FIGURE 1. Intravital imaging maintains intact blood flow without damaging the pancreas. (**A**) Setup for intravital two-photon pancreas imaging. A heated suction window stabilizes the surgically exposed pancreas for imaging. (**B** and **C**) Representative maximum intensity projection images of islets imaged intravitally through the suction imaging window captured using two-photon microscopy. Vascular space is labeled with 70-kDa dextran-rhodamine (red). Images are representative of seven experiments. (B) Islets are identifiable by their dense convoluted vasculature compared with exocrine tissue vasculature. The border of the islet is identified with a yellow dashed line. Scale bar, 30 μm. (C) NOD mouse islet with transferred BDC-2.5 T cells (green). The collagen fluorescence is provided by the second harmonic (blue), which demonstrates that the T cell infiltration is inside the islet basement membrane. Scale bar, 100 μm. (**D**) Neutrophils do not accumulate at the site of imaging. Fluorescently labeled neutrophils were transferred into mice prior to surgical exposure and imaging of the pancreas through the suction window. The number of neutrophils was counted every 90 s. The lack of neutrophil accumulation shows that the imaging site was not damaged during imaging. Data are representative of one islet per mouse in three experiments. (**E**) Suction imaging window does not impede blood flow. Fluorescent beads were tracked within blood vessels of different diameter within and around the pancreatic islets. Each dot represents one bead. Data are representative of three islets per mouse in two experiments.

100% oxygen) (VetOne). A total of 250–500 μg 70-kDa dextran-rhodamine (Invitrogen) or Evans blue (Sigma-Aldrich) was injected i.v. to label the vasculature. Skin was removed above the surgical area, and a semicircular flap of the peritoneal wall was cut to expose the pancreas. The pancreas was manipulated with saline-soaked swabs, and the area was sealed with plastic wrap to prevent tissue desiccation, damage, and evaporative heat loss. The mouse was hydrated with s.c. saline and maintained at 37°C using a homeothermic warmer (Kent Scientific). The suction imaging window (26) was heated to 35–37°C and affixed using a vacuum of 25–40 mmHg to immobilize the pancreas for imaging. Islets were identified using the distinct vasculature pattern present within islets (13) (Supplemental Fig. 1). Islets that were largely destroyed lacked the distinctive vasculature pattern and were excluded from analysis. One to five islets per mouse were imaged from seven mice for 16 total islets in seven independent experiments.

Explanted islet isolation

Islets were isolated, as previously described (9, 11). Briefly, mice were anesthetized with ketamine/xylazine prior to cervical dislocation. The pancreas was inflated with ~3 ml 0.8 mg/ml collagenase P (Roche) and 10 μg/ml DNase I (Roche) in HBSS (Cellgro) via the common bile duct. Following inflation, the pancreas was removed and incubated at 37°C for 10–11 min, and the islets were isolated by Histopaque (Sigma-Aldrich) density centrifugation. To ensure that the islets were intact, they were handpicked under a dissecting microscope. Isolated islets were embedded in 3% low melting temperature agarose (Fisher) in Dulbecco's PBS. During imaging, islets were maintained at 35–37°C with flow of 95% O_2/5% CO_2 saturated RPMI 1640 (Life Technologies).

T cell preparation and imaging

Spleen and lymph node cells from female BDC-2.5 mice were stimulated in vitro with 1 μg/ml BDC-2.5 mimetope (YVRPLWVRME) (π Proteomics). For studies using both BDC-2.5 and BDC-6.9 T cells, T cell stimulation was performed in vitro using 1 μg/well plate-bound anti-CD3 (Bio-XCell) and 2 μg/ml soluble anti-CD28 (Bio-XCell) Abs. Cells were maintained in media containing 10 IU/ml human rIL-2 (27) (AIDS Research and Reference Reagent Program, Division of AIDS, National Institute of Allergy and Infectious Diseases, National Institutes of Health, from M. Gately, Hoffmann-La Roche). Day 6–14 postactivation, T cells were labeled with Violet Proliferation Dye 450 (BD Biosciences), CFSE (Invitrogen), CMTMR (Invitrogen), or Cell Proliferation Dye (eFluor670) (eBioscience). A total of 5×10^6 and 1×10^7 labeled cells was transferred i.v. via the tail 48 and 24 h prior to imaging, respectively, for motility studies. For studies using only BDC-2.5 T cells transferred into wild-type (WT) NOD recipients, three to five islets per mouse were imaged from four mice for 16 total islets in three independent experiments. For studies using BDC-2.5 and BDC-6.9 cotransfers, 5×10^6 peptide-stimulated BDC-2.5 T cells were transferred 48 h prior to imaging to establish islet infiltration levels. Twenty-four hours prior to imaging, 1×10^7 Ab-stimulated BDC-2.5 and BDC-6.9 T cells were cotransferred. For WT recipients, 3–10 islets per mouse were imaged from four mice for 25 total islets in four independent experiments. For NOD.C6 recipients, 4–6 islets per mouse were imaged from five mice for 25 total islets in five independent experiments. An Olympus FV1000MPE two-photon microscope (28) was used for imaging T cells in the islets. Excitation was performed at 810 nm. Imaging fields were as described (28). Images of 27–53 *xy* planes with 3-μm *z*-spacing were acquired every minute for 30 min.

Interaction imaging

$CD4^+$ T cells from NOD.BDC-2.5 mice were selected using a negative selection kit (Stemcell). A total of 5×10^6 dye-labeled T cells was adoptively transferred i.v. into female NOD.CD11c-YFP recipient mice ages 9–18 wk old. Twenty-four hours after transfer, islets were isolated and imaged, as described above. Two to six islets per mouse were imaged from five mice for 15 total islets in five independent experiments.

Neutrophil and bead transfer and imaging

A custom-built two-photon microscope with published specifications (29) was used for imaging neutrophils and beads in the islets.

Neutrophils were isolated from bone marrow using a Percoll (Sigma-Aldrich) gradient, labeled with CMTMR (Invitrogen), and transferred retro-orbitally into B6.MIP-GFP mice immediately prior to surgery and imaging. Excitation was performed at 800 nm on a 3 × 3 area of adjacent *z*-stacks around a representative islet. Images of up to 25 *xy* planes with 5- to 6-μm *z*-spacing were acquired every 90 or 120 s for 2–3 h.

Fluorescent beads (1.75 μm; Invitrogen) were i.v. injected into B6.MIP-GFP mice at the time of imaging. Imaging was performed at a wavelength of 800 nm on a single *xyz* plane at a rate of 30 frames per second.

Analysis

Image analysis of cells and beads was performed using Imaris (Bitplane) and MATLAB (Mathworks). Images were linearly unmixed, as previously described (29). To determine the level of islet infiltration, the region with visible transferred fluorescent T cells was manually drawn in each *z* plane, and a total volume was determined. The infiltrated volume was then used to determine the percentage of the total islet volume that had been infiltrated. Islets were grouped into islets with mild infiltration (<30% of islet volume infiltrated) and advanced infiltration (between 30 and 60% of islet volume infiltrated). Cells within the islets tracked for ≥5 min were used to obtain speed, arrest coefficient, and track straightness. Cells tracked for ≥10 min within the islets were used to determine mean squared displacement. T cell–APC contacts were defined as a T cell and $CD11c^+$ cell spending ≥2 min with their cell surfaces within 1 μm of each other. Sustained interactions were defined as ≥10-min duration of contact. Statistics were calculated with Prism software (GraphPad).

Results

Immune cell dynamics in live islets can be analyzed by two imaging methods

Our goal was to analyze T cell behavior, including motility and interactions, during the progression of islet destruction in T1D. To do so, we validated two methods for imaging live intact pancreatic islets by two-photon microscopy: explanted islet imaging and a novel method of intravital islet imaging. Using these techniques, we analyzed T cell motility in the islets of NOD mice, a spontaneous model of T1D. Fluorescently labeled, activated, BDC-2.5 $CD4^+$ T cells (24) were transferred into NOD mice 24 and 48 h before islet imaging. Data from the 24-h T cell transfer are reported and representative of both transferred populations.

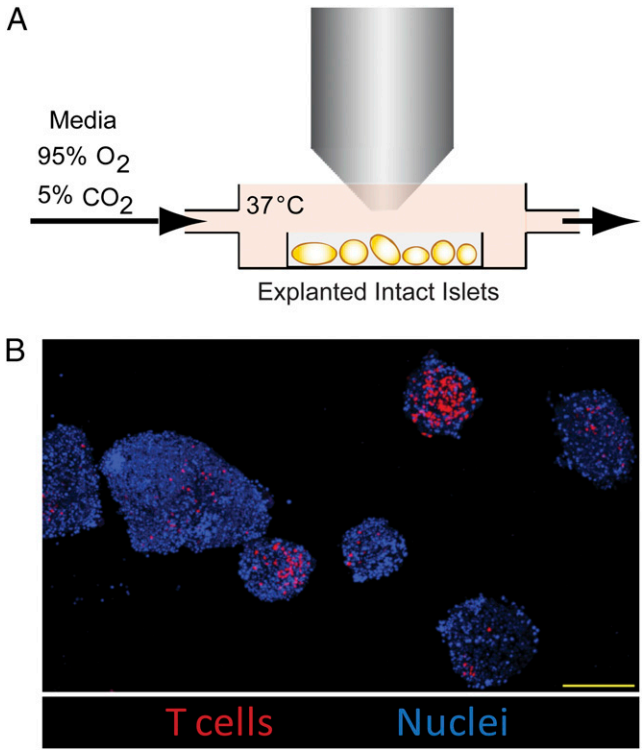

FIGURE 2. Explanted islet imaging allows high resolution, high throughput imaging. (**A**) Setup of explanted islet two-photon imaging. Isolated pancreatic islets were mounted in low melting temperature agarose and maintained at 35–37°C with constant flow of oxygenated media. (**B**) Representative multiple field image of explanted islets. BDC-2.5 T cells (red) were transferred into WT NOD recipients, and islets were isolated. Image shows a maximum intensity projection of explanted islets. Nuclei are labeled with Hoechst 33342 (blue). Scale bar, 200 μm. Images are representative of >3 experiments.

Intravital imaging allows the study of T cell behavior in vivo without damaging the pancreas or affecting blood flow. The pancreas was surgically exposed via a semicircular incision through the skin and peritoneum. To stabilize the surgically exposed pancreas, we reversibly adhered an imaging window (26) to the pancreas with gentle suction and heated the window to 35˚C–37˚C (Fig. 1A). This relatively simple procedure maintained the stability required for imaging with minimal force applied to the pancreas. This technique is significantly less invasive than previously established procedures for intravital pancreas imaging (13, 17).

The islets were distinguished from the exocrine tissue based on the characteristic dense, convoluted islet vasculature (13) compared with the looser, mesh-like exocrine tissue vasculature (Fig. 1B). We confirmed that, as previously reported (13), this vasculature morphology was associated specifically with islets, by examining the islet vascular morphology in the MIP-GFP β cell reporter mice (Supplemental Fig. 1). A collagen-rich basement membrane that surrounds the islets breaks down with advanced insulitis (30). We were able to visualize peri-insulitic T cell infiltration inside the collagen of the intact basement membrane (Fig. 1C).

Damage to the pancreas can lead to local and systemic inflammation (31). Previous studies using other methods of intravital pancreas imaging did not determine whether manipulation of the pancreas induced damage or inflammation. To determine whether our imaging technique induced tissue damage, we assessed neutrophil accumulation at the imaging site (Fig. 1D, Supplemental Video 1). The absence of neutrophil accumulation suggests that the pancreas remained undamaged during our imaging time frame. To determine whether blood flow was impeded by the application of the suction imaging window, we also imaged fluorescent bead motility through the blood vessels. Blood flow rates were similar to flow rates reported within the mouse pancreas (13, 32), indicating that the blood flow through the islets was unimpeded by our intravital imaging technique (Fig. 1E, Supplemental Video 2).

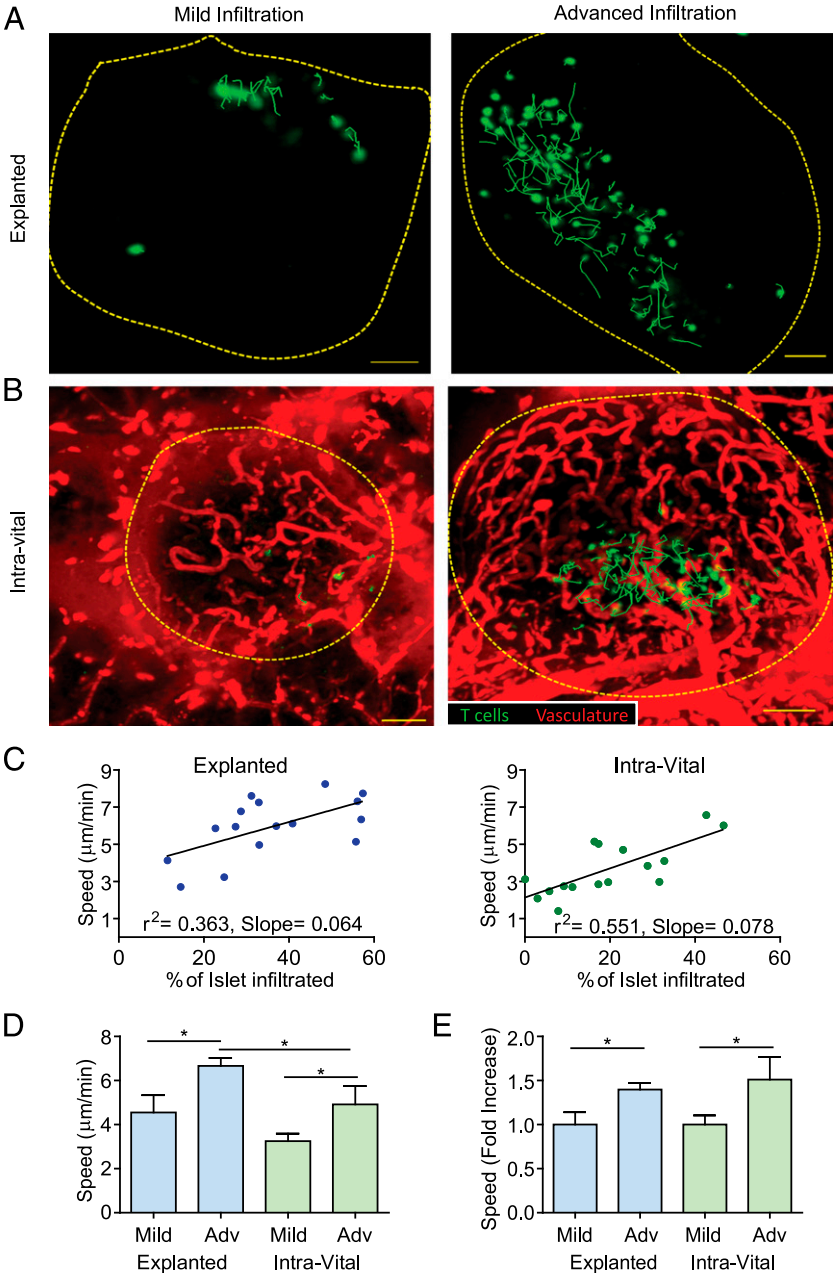

FIGURE 3. T cell motility increases with progression of islet infiltration. (**A** and **B**) Activated BDC-2.5 T cells (green) were fluorescently labeled and transferred 24 h prior to imaging. Representative maximum intensity projection images from explanted (A) or intravital (B) islets captured using two-photon microscopy. Dashed lines represent the islet border. Green lines represent 10-min paths of BDC-2.5 T cell movement. Images are representative of islets with mild infiltration (<30% of islet volume infiltrated) or advanced infiltration (30–60% of islet volume infiltrated). Scale bars, 50 μm. (**C**–**E**) Quantification of T cell motility within explanted or intravital islets. Data pooled from 16 explanted islets from four mice in three independent experiments and 16 intravital islets from seven mice in seven independent experiments. $*p < 0.05$, measured by Student *t* test. (C) Linear correlation of the average T cell velocity within an islet versus the percentage of the infiltrated islet volume. Each dot represents the average of all of the tracked T cells within a single islet. (D and E) Average of individual islets. (D) T cell crawling speed in explanted versus intravital islets. (E) Fold increase in crawling speed between islets with mild and advanced infiltration.

Imaging intact explanted islets enables analysis of large numbers of islets. Live explanted islet imaging has not been validated to ensure that T cell behavior in the explants reflects T cell activity within the intact pancreas. Isolated islets were embedded in low melt agarose and maintained at 35˚C–37˚C with flow of warmed oxygenated media (Fig. 2A). Effective islet imaging was dependent upon maintaining intact islets throughout the isolation and imaging process, and was ensured by careful control of digestion time and handpicking of intact islets under a dissecting microscope (Fig. 2B). This technique allowed us to image large numbers of islets from each mouse.

T cell motility increases as islet infiltration increases

The rate of T cell motility and arrest within tissues can be used to determine whether T cells are likely to be interacting with APCs or target cells, resulting in T cell signaling. Thus, using adoptively transferred BDC2.5 T cells, T cell motility was measured within the islets to determine when T cells were likely to be receiving antigenic signals during islet infiltration (Fig. 3). Additionally, using i.v. 70-kDa dextran to label the blood volume, we observed vascular leakage surrounding some infiltrated islets (Fig. 3B), which has been shown to be a prognostic indicator of pathogenic infiltration (33).

Our analysis demonstrated a correlation between T cell crawling speed and degree of islet infiltration (Fig. 3C, 3D). Therefore, to understand how progression of islet infiltration affected T cell behavior within the islets, we categorized islets based on stage of islet infiltration. Islets were categorized as having mild (<30% of islet volume infiltrated) or advanced (30–60% of islet volume infiltrated) infiltration (Fig. 3A, 3B). Islets exhibiting both infiltration levels were found within the same animal, demonstrating the heterogeneity of the islet infiltration. T cell behavior differed between individual islets of the same animal, but correlated with the degree of islet infiltration.

Significant differences in T cell motility existed between mild and advanced islet infiltration (Fig. 3D, 3E, Supplemental Videos 3–6). Although there were small differences in crawling speed between the two imaging methods, the change in T cell behavior, indicated by the fold increase in T cell speed between mild and advanced islets, was comparable (Fig. 3E). Cellular confinement is measured in part by T cell track straightness, which was consistent between the explanted and intravital imaging methods. However, track straightness was increased in advanced versus mild infiltrated islets, suggesting that T cells were less confined and/or they had increased directional motility with increased infiltration (Fig. 4A). Analysis of T cell arrest by the arrest coefficient (percentage of time T cell speed is <2 μm/min) showed that T cells in advanced islet infiltration arrested less than T cells in mild islet infiltration (Fig. 4B). The change in arrest coefficient resulted from an increased percentage of cells that were arrested for a long period of time in islets with mild infiltration (Fig. 4C), possibly due to interactions with APCs. A T cell's ability to move away from its point of origin can be analyzed by the mean squared displacement (MSD) over time. After 5 min, there were significant differences in the MSD between mild and advanced islet infiltration for both explanted and intravitally imaged islets (Fig. 4D).

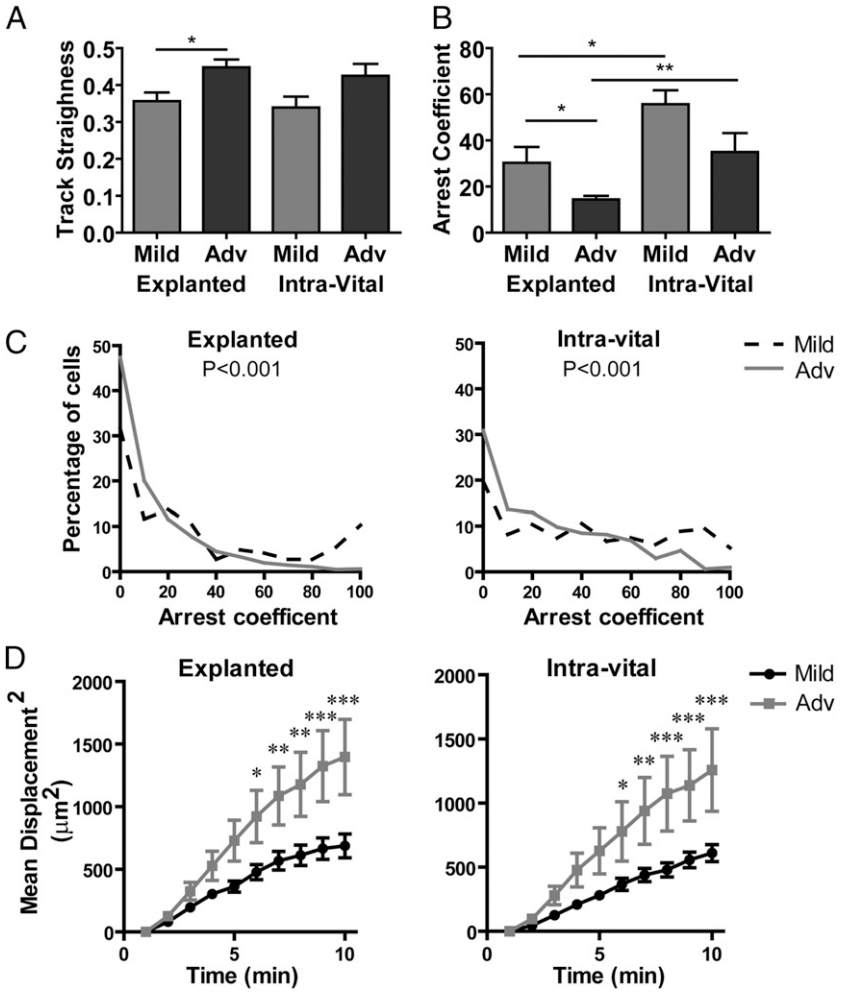

FIGURE 4. T cells reduce arrest and increase displacement as islet infiltration progresses. Activated BDC-2.5 T cells were fluorescently labeled and transferred 24 h prior to imaging, as in Fig. 3. Data were pooled from 16 explanted islets from four mice in three independent experiments and 16 intravital islets from seven mice in seven independent experiments. (**A** and **B**) Average of individual islets. (A) T cell track straightness (1 = cell moves in a straight line). (B and **C**) T cell arrest coefficient (% of time crawling speed is <2 μm/min). (**D**) Mean squared displacement (μm^2) over time. $*p < 0.05$, $**p < 0.01$, $***p < 0.001$; measured by two-way ANOVA with Bonferroni posttests or Student *t* test.

In contrast, there was no significant difference in the MSD when comparing the intravital versus explanted methods (Supplemental Fig. 2).

The changes in T cell motility with progressing islet infiltration suggest that the islet environment is an important factor in T cell behavior in the islets. The difference in absolute speed (Fig. 3C, 3D) and arrest coefficient (Fig. 4B, 4C) between the two methods may be due to differences in available oxygen (34). However, this did not affect the biological change in T cell motility (Fig. 3E) or the ability of T cells to translocate (Fig. 4D). These data demonstrate that the environmental factors that drive these biological changes are maintained with both imaging techniques. These data validate explanted islet imaging as a technique to examine cellular motility and interactions within the islet.

The presence of islet Ag drives T cell arrest early in islet infiltration

Based on these data and our previous data (9), it was clear that environmental factors play a critical role in the behavior of T cells in the islets as infiltration progresses; however, the environmental changes driving the observed behaviors have not been elucidated. We therefore examined the presence of specific Ag as a potential environmental factor governing T cell behavior within the islets. To determine whether the presence of T cell Ag was important for the arrest (Fig. 4B, 4C) and slow motility (Fig. 3D) observed in mild islet infiltration, we analyzed NOD.BDC-6.9 TCR transgenic (25) T cells in the NOD.C6 mouse. The NOD.C6 mouse contains a portion of the BALB/c mouse chromosome 6, which lacks the Ag for the BDC-6.9 T cell clone (35) used to generate the NOD.BDC-6.9 TCR transgenic (25), whereas WT NOD chromosome 6 contains the Ag. The NOD.C6 mouse has normal islet infiltration and diabetes incidence, but the NOD.C6.BDC-6.9 has no disease progression (25). Utilizing the NOD.C6 as a recipient mouse, we cotransferred in both BDC-2.5 T cells (for which Ag was present) and BDC-6.9 T cells (for which Ag was absent). This allowed us to determine how the presence of specific Ag affects T cell motility and arrest in the islet environment.

In WT NOD mice, BDC-6.9 T cells exhibited slower motility than BDC-2.5 T cells, but showed a similar increase in motility as infiltration increased (Fig. 5A). The slower BDC-6.9 T cell motility could be due either to higher levels of Ag for the BDC-6.9 T cells in the islets or to a higher affinity TCR for the presented Ag. However, in the NOD.C6 in which the Ag for BDC-6.9 T cells was absent, BDC-6.9 T cells had higher motility compared with BDC-2.5 T cells in the same islet environment (Fig. 5B). BDC-2.5 T cells had similar motility in islets from both WT NOD and NOD.C6, demonstrating that the islet environments were similar, whereas BDC-6.9 had faster motility when their Ag was absent in the NOD.C6 islets compared with WT NOD islets (Supplemental Fig. 3).

Comparing the ratio of BDC-6.9/BDC-2.5 T cell motility within the same islet shows that in very mild infiltration (0–5% infiltrated) and advanced infiltration (30–60% infiltrated), both populations of T cells moved at similar velocities regardless of the presence of specific Ag. Notably, under conditions of very mild infiltration, the T cells were largely arrested, most likely due to physical confinement. In contrast, in advanced states of infiltration, the T cells were moving quickly regardless of Ag presence.

Significantly, in islets with mild infiltration (5–30%), infiltrating BDC-6.9 T cells (No Ag) increased crawling velocity compared with BDC-2.5 T cells (+Ag) within the same islet (Fig. 5C). This difference in motility in mild islet infiltration is due to a decrease in BDC-6.9 T cell (No Ag) arrest (Fig. 5D). The decreased BDC-6.9 arrest demonstrates that the presence of Ag is a major environmental factor that governs T cell behavior at early stages of islet infiltration.

T cell–APC interaction duration is reduced with increased islet infiltration

To determine whether the Ag-dependent arrest in mild islet infiltration was due to interactions with CD11c$^+$ APCs, T cell–APC interactions were analyzed in explanted islets by two-photon microscopy (Fig. 6). Fluorescently labeled BDC-2.5 T cells were

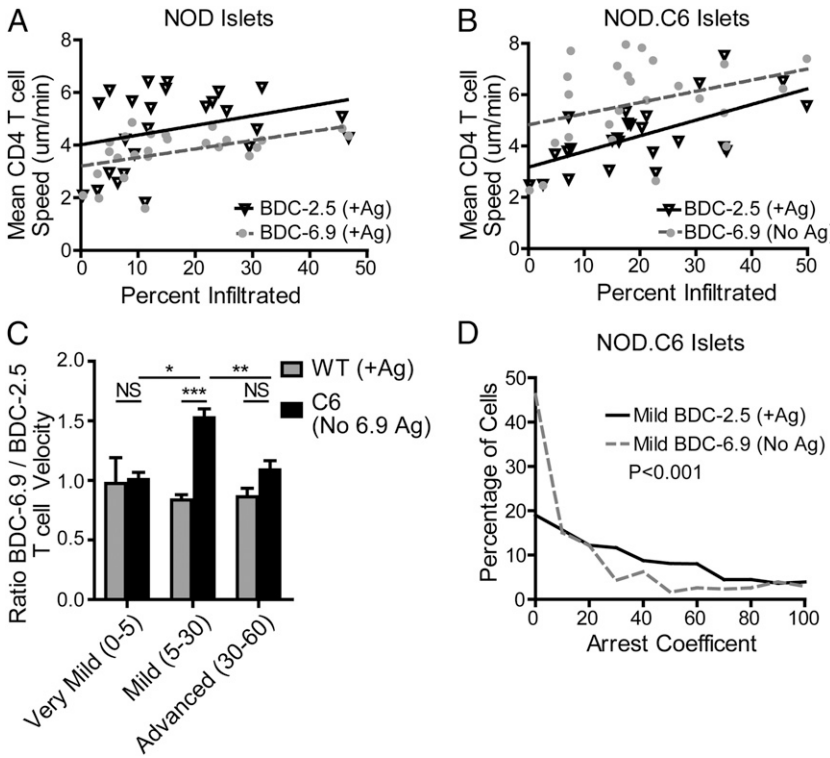

FIGURE 5. Early T cell arrest is Ag dependent. BDC-2.5 T cells were fluorescently labeled and transferred into WT NOD or NOD.C6 recipient mice 48 h prior to imaging to determine infiltration state. BDC-6.9 T cells and BDC-2.5 T cells were cotransferred 24 h prior to imaging to determine T cell motility. The Ag for BDC-6.9 T cells is absent in the NOD.C6 recipients. Data represent 25 WT islets from four mice in four experiments and 25 NOD.C6 islets from five mice in five experiments. Each point represents the average T cell motility within one islet. (**A**) In WT NOD islets in which the Ag was present for BDC-2.5 and BDC-6.9 T cells, both types of T cells increase motility at a similar rate as islet infiltration increases. (**B**) In NOD.C6 islets, in which the Ag is present for BDC-2.5 T cells, but absent for BDC-6.9 T cells, the BDC-6.9 T cells move faster in the absence of their Ag. (**C**) The ratio of average BDC-6.9 T cell motility to the average BDC-2.5 T cell motility within the same islet. Infiltration states: very mild (0–5%), mild (5–30%), and advanced (30–60%). (**D**) Comparison of the arrest coefficient of all BDC-2.5 and BDC-6.9 T cells within islets with mild infiltration. BDC-6.9 T cells (No Ag) have reduced arrest. $*p < 0.05$, $**p < 0.01$, $***p < 0.001$ by two-tailed Student t test.

transferred into NOD.CD11c-YFP recipient mice. We analyzed the frequency and duration of T cells that contacted CD11c$^+$ APCs in the islets. Sustained interactions, lasting at least 10 min (Fig. 6A, Supplemental Video 7), or transient brief interactions (Fig. 6B, Supplemental Video 8) were present in islets with both mild and advanced infiltration. Although the percentage of T cells that contacted a CD11c$^+$ APC was slightly reduced in islets with advanced infiltration (Fig. 6C), this was not significant. However, the percentage of contacts that resulted in sustained interactions (≥10-min contact) was significantly greater in islets with mild infiltration (Fig. 6D). Additionally, the duration of T cell–APC contacts was significantly reduced in islets with advanced infiltration, further supporting the loss of sustained T cell–APC interactions (Fig. 6E). These data suggest that T cells are receiving antigenic restimulation from CD11c$^+$ APCs in islets with mild infiltration, but that these interactions along with antigenic stimulation are lost in islets with advanced infiltration.

Discussion

The data presented in this work in the spontaneously autoimmune NOD model of T1D show that early in islet infiltration, Ag-dependent T cell arrest occurs, and is due at least in part to antigenic interactions with CD11c$^+$ APCs. As islet infiltration progresses, these Ag-dependent sustained interactions with APCs are lost, and T cell behavior is governed by factors other than Ag. We analyzed T cells from a single adoptive transfer; however, varying degrees of endogenous autoimmune islet infiltrate were present within individual islets. T cell behavior within an animal was governed by the individual islet environment rather than the overall state of disease within the animal or the time spent within an islet. This highlights the importance of the individual islet environment in controlling T cell behavior within the islets, including factors such as Ag presentation and the chemokine and cytokine milieu.

Changes in the T cell response with T1D disease progression were not examined by the work of others studying the dynamics of

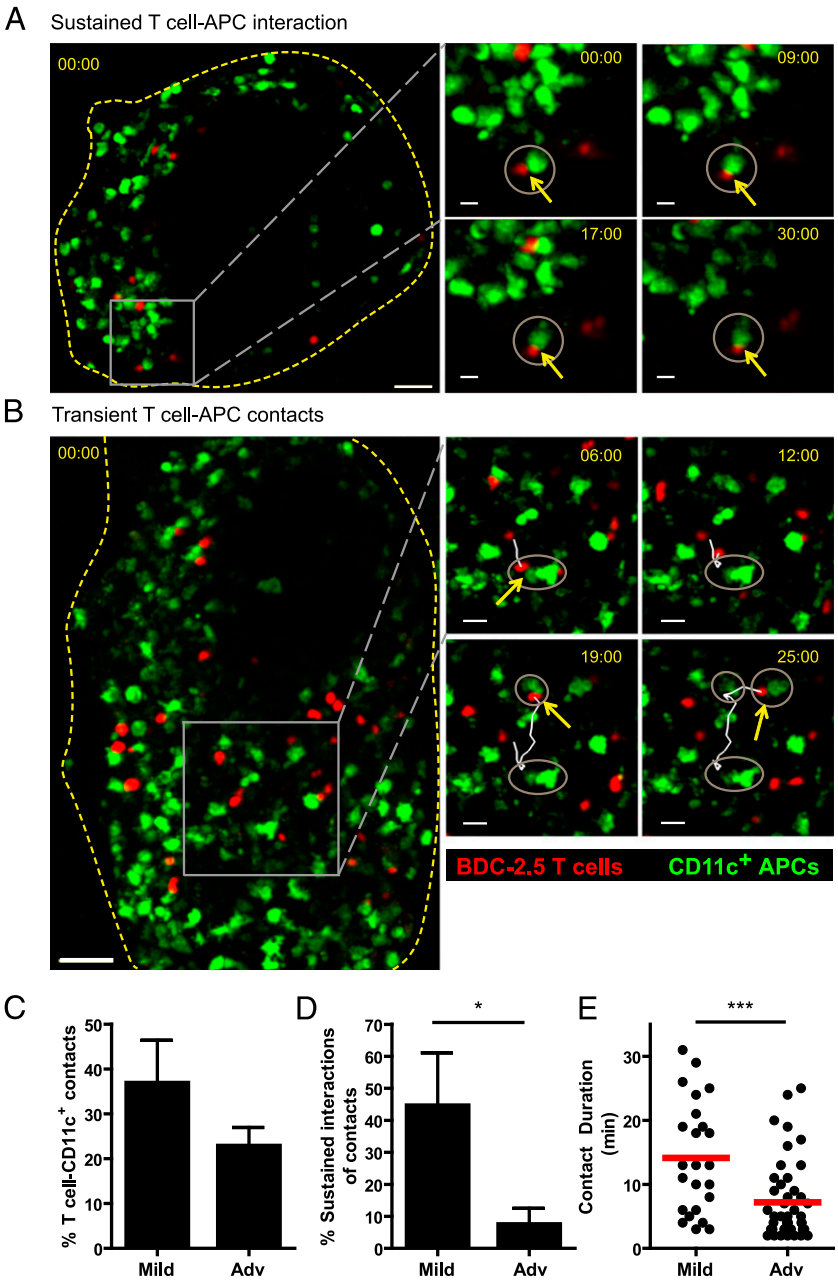

FIGURE 6. Sustained T cell–CD11c$^+$ APC interactions are lost with progression of islet infiltration. Fluorescently labeled BDC-2.5 T cells were transferred into CD11c-YFP hosts 24 h prior to islet isolation and imaging. Data represent 15 islets from five mice in five independent experiments. (**A** and **B**) Maximum intensity projection images showing BDC-2.5 (red) and CD11c$^+$ APCs (green) within pancreatic islets. Yellow box indicates the region shown in time-lapse images on the *right*. Gray circles highlight the CD11c$^+$ APCs that the T cell of interest has contacted; yellow arrows show current T cell–APC contacts. Time stamps = min:s. (A) Sustained T cell–APC interaction in an islet with mild infiltration. Scale bar, 40 μm for whole islet and 10 μm for time-lapse images. (B) Transient T cell contacts with different CD11c$^+$ APCs in an islet with advanced infiltration. Scale bar, 50 μm for whole islet and 20 μm for time-lapse images. (**C**) Average percentage of T cells within individual islets that contact CD11c$^+$ APCs for at least 2 min. (**D**) Average percentage of T cells that contacted CD11c$^+$ APCs, which had sustained interactions of ≥10 min. (**E**) Duration of T cell– CD11c$^+$ APC contacts. *$p < 0.001$, ***$p < 0.001$ by two-tailed Student *t* test.

the T cell response in the islets (12, 15, 17, 22). Our findings showing changes in T cell behavior with progression of infiltration are significant in two ways. First, they suggest that antigenic T cell interactions with APCs in the islets are present in the early stages of infiltration. It is likely that these T cell interactions lead to expression of effector functions (9, 10), which promote inflammation and drive entry of other cells into the islets (12, 36). Secondly, the lack of Ag recognition in the islets with increased infiltration suggests that autoimmune T cell response in the islets may be at least temporarily dampened during the course of islet infiltration and disease progression. These data are in agreement with results analyzing the OT-I T cell response in RIP-mOva islets (9). However, tolerance is re-established in the RIP-mOva model, so we were surprised to consistently find the same behavior in the islets of female NOD mice, considering that the incidence of disease is 75% by 40 wk in our colony.

There are several potential explanations for why T cells lose antigenic interactions with progression of islet infiltration. Because transient T cell–APC interactions result in tolerance induction in lymph nodes (19, 21, 22), it is possible that similar tolerance mechanisms occur within the islets, and this behavior represents the establishment of tolerance. Alternatively, T cells may have completed interactions with APCs and no longer require restimulation. However, data in the RIP-mOva model suggest that effector cytokine production is lost along with restimulation, suggesting that a requirement may still be present. Other possibilities include that Ag levels on APCs may be below a stimulatory threshold or the APC populations change (9) and those present within the islets are no longer able to support sustained interactions. Increased chemokine expression with islet infiltration (36) may also contribute to increased T cell motility, particularly in advanced islet infiltration in which Ag presence has a reduced effect on T cell motility.

The correlation between T cell behavioral changes and islet infiltration levels in both explanted and intravital imaging validates these techniques for analyzing immune cell dynamics within the islets. Explanted islet imaging is a higher throughput technique that allows for the use of lower intensity fluorescent reporters. As we have shown previously, this can allow reporters such as biosensors to dynamically indicate effector function or signaling to be analyzed within the islets (9). Intravital imaging allows us to investigate processes such as T cell entry into the islets (18) from the vasculature and vascular leakage, which are processes that require intact blood flow and vascular structure. Our intravital imaging technique also allows for the identification of the islets based on the vascular morphology, eliminating the need for a fluorescent β cell reporter such as MIP-GFP. Examining T cell motility within islets of MIP-GFP mice is challenging because the bright signal can obscure other fluorescent cells. Eliminating the need for such reporters allows for imaging within the interior of intact islets using both of our imaging methods. By validating that both techniques provide the same readout of T cell motility at different stages of infiltration, we are able to use the techniques for their best application.

The lack of effective treatments to halt the autoimmune response in patients with T1D may be in part due to differences in efficacy of treatment within islets at different stages of infiltration present within the same patient. This heterogeneity may leave a portion of the autoimmune response untreated in these patients. The imaging studies we present in this work and the studies of others (37) demonstrate the importance of examining islets on an individual basis. Examination of the heterogeneous response within the entire pancreas may hide important differences in immune response at different stages of islet infiltration. Using our imaging techniques in models of T1D, we can examine differences in T cell effector functions and activation state at different stages of disease. This approach may generate insights into the effects of therapeutic treatments and mechanisms of peripheral tolerance at different stages of the disease progression.

Acknowledgments

We thank Jason Lilly for islet isolation, Brianna Traxinger for animal husbandry and genotyping, and Scott Thompson for editing of the manuscript.

Disclosures

The authors have no financial conflicts of interest.

References

1. Gagnerault, M.-C., J. J. Luan, C. Lotton, and F. Lepault. 2002. Pancreatic lymph nodes are required for priming of beta cell reactive T cells in NOD mice. *J. Exp. Med.* 196: 369–377.
2. Bluestone, J. A., K. Herold, and G. Eisenbarth. 2010. Genetics, pathogenesis and clinical interventions in type 1 diabetes. *Nature* 464: 1293–1300.
3. Driver, J. P., D. V. Serreze, and Y.-G. Chen. 2011. Mouse models for the study of autoimmune type 1 diabetes: a NOD to similarities and differences to human disease. *Semin. Immunopathol.* 33: 67–87.
4. Jansen, A., F. Homo-Delarche, H. Hooijkaas, P. J. Leenen, M. Dardenne, and H. A. Drexhage. 1994. Immunohistochemical characterization of monocytes-macrophages and dendritic cells involved in the initiation of the insulitis and beta-cell destruction in NOD mice. *Diabetes* 43: 667–675.
5. Penaranda, C., Q. Tang, N. H. Ruddle, and J. A. Bluestone. 2010. Prevention of diabetes by FTY720-mediated stabilization of peri-islet tertiary lymphoid organs. *Diabetes* 59: 1461–1468.
6. Prochazka, M., D. V. Serreze, W. N. Frankel, and E. H. Leiter. 1992. NOR/Lt mice: MHC-matched diabetes-resistant control strain for NOD mice. *Diabetes* 41: 98–106.
7. Tang, Q., J. Y. Adams, A. J. Tooley, M. Bi, B. T. Fife, P. Serra, P. Santamaria, R. M. Locksley, M. F. Krummel, and J. A. Bluestone. 2006. Visualizing regulatory T cell control of autoimmune responses in nonobese diabetic mice. *Nat. Immunol.* 7: 83–92.
8. Ott, P. A., M. R. Anderson, M. Tary-Lehmann, and P. V. Lehmann. 2005. CD4+CD25+ regulatory T cells control the progression from periinsulitis to destructive insulitis in murine autoimmune diabetes. *Cell. Immunol.* 235: 1–11.
9. Friedman, R. S., R. S. Lindsay, J. K. Lilly, V. Nguyen, C. M. Sorensen, J. Jacobelli, and M. F. Krummel. 2014. An evolving autoimmune microenvironment regulates the quality of effector T cell restimulation and function. *Proc. Natl. Acad. Sci. USA* 111: 9223–9228.
10. Chee, J., H. J. Ko, A. Skowera, G. Jhala, T. Catterall, K. L. Graham, R. M. Sutherland, H. E. Thomas, A. M. Lew, M. Peakman, et al. 2014. Effector-memory T cells develop in islets and report islet pathology in type 1 diabetes. *J. Immunol.* 192: 572–580.
11. Melli, K., R. S. Friedman, A. E. Martin, E. B. Finger, G. Miao, G. L. Szot, M. F. Krummel, and Q. Tang. 2009. Amplification of autoimmune response through induction of dendritic cell maturation in inflamed tissues. *J. Immunol.* 182: 2590–2600.
12. Calderon, B., J. A. Carrero, M. J. Miller, and E. R. Unanue. 2011. Cellular and molecular events in the localization of diabetogenic T cells to islets of Langerhans. *Proc. Natl. Acad. Sci. USA* 108: 1561–1566.
13. Nyman, L. R., K. S. Wells, W. S. Head, M. McCaughey, E. Ford, M. Brissova, D. W. Piston, and A. C. Powers. 2008. Real-time, multidimensional in vivo imaging used to investigate blood flow in mouse pancreatic islets. *J. Clin. Invest.* 118: 3790–3797.
14. Speier, S., D. Nyqvist, O. Cabrera, J. Yu, R. D. Molano, A. Pileggi, T. Moede, M. Köhler, J. Wilbertz, B. Leibiger, et al. 2008. Noninvasive in vivo imaging of pancreatic islet cell biology. *Nat. Med.* 14: 574–578.
15. Abdulreda, M. H., G. Faleo, R. D. Molano, M. Lopez-Cabezas, J. Molina, Y. Tan, O. A. Echeverria, E. Zahr-Akrawi, R. Rodriguez-Diaz, P. K. Edlund, et al. 2011. High-resolution, noninvasive longitudinal live imaging of immune responses. *Proc. Natl. Acad. Sci. USA* 108: 12863–12868.
16. Mojibian, M., B. Harder, A. Hurlburt, J. E. Bruin, A. Asadi, and T. J. Kieffer. 2013. Implanted islets in the anterior chamber of the eye are prone to autoimmune attack in a mouse model of diabetes. *Diabetologia* 56: 2213–2221.
17. Coppieters, K., N. Amirian, and M. von Herrath. 2012. Intravital imaging of CTLs killing islet cells in diabetic mice. *J. Clin. Invest.* 122: 119–131.
18. Jacobelli, J., R. S. Lindsay, and R. S. Friedman. 2013. Peripheral tolerance and autoimmunity: lessons from in vivo imaging. *Immunol. Res.* 55: 146–154.
19. Hugues, S., L. Fetler, L. Bonifaz, J. Helft, F. Amblard, and S. Amigorena. 2004. Distinct T cell dynamics in lymph nodes during the induction of tolerance and immunity. *Nat. Immunol.* 5: 1235–1242.
20. Shakhar, G., R. L. Lindquist, D. Skokos, D. Dudziak, J. H. Huang, M. C. Nussenzweig, and M. L. Dustin. 2005. Stable T cell-dendritic cell interactions precede the development of both tolerance and immunity in vivo. *Nat. Immunol.* 6: 707–714.
21. Katzman, S. D., W. E. O'Gorman, A. V. Villarino, E. Gallo, R. S. Friedman, M. F. Krummel, G. P. Nolan, and A. K. D. Abbas. 2010. Duration of antigen

receptor signaling determines T-cell tolerance or activation. *Proc. Natl. Acad. Sci. USA* 107: 18085–18090.
22. Fife, B. T., K. E. Pauken, T. N. Eagar, T. Obu, J. Wu, Q. Tang, M. Azuma, M. F. Krummel, and J. A. Bluestone. 2009. Interactions between PD-1 and PD-L1 promote tolerance by blocking the TCR-induced stop signal. *Nat. Immunol.* 10: 1185–1192.
23. Lindquist, R. L., G. Shakhar, D. Dudziak, H. Wardemann, T. Eisenreich, M. L. Dustin, and M. C. Nussenzweig. 2004. Visualizing dendritic cell networks in vivo. *Nat. Immunol.* 5: 1243–1250.
24. Katz, J. D., B. Wang, K. Haskins, C. Benoist, and D. Mathis. 1993. Following a diabetogenic T cell from genesis through pathogenesis. *Cell* 74: 1089–1100.
25. Pauza, M. E., C. M. Dobbs, J. He, T. Patterson, S. Wagner, B. S. Anobile, B. J. Bradley, D. Lo, and K. Haskins. 2004. T-cell receptor transgenic response to an endogenous polymorphic autoantigen determines susceptibility to diabetes. *Diabetes* 53: 978–988.
26. Looney, M. R., E. E. Thornton, D. Sen, W. J. Lamm, R. W. Glenny, and M. F. Krummel. 2011. Stabilized imaging of immune surveillance in the mouse lung. *Nat. Methods* 8: 91–96.
27. Lahm, H. W., and S. Stein. 1985. Characterization of recombinant human interleukin-2 with micromethods. *J. Chromatogr. A* 326: 357–361.
28. McKee, A. S., M. A. Burchill, M. W. Munks, L. Jin, J. W. Kappler, R. S. Friedman, J. Jacobelli, and P. Marrack. 2013. Host DNA released in response to aluminum adjuvant enhances MHC class II-mediated antigen presentation and prolongs CD4 T-cell interactions with dendritic cells. *Proc. Natl. Acad. Sci. USA* 110: E1122–E1131.
29. Bullen, A., R. S. Friedman, and M. F. Krummel. 2009. Two-photon imaging of the immune system: a custom technology platform for high-speed, multicolor tissue imaging of immune responses. *Curr. Top. Microbiol. Immunol.* 334: 1–29.
30. Irving-Rodgers, H. F., A. F. Ziolkowski, C. R. Parish, Y. Sado, Y. Ninomiya, C. J. Simeonovic, and R. J. Rodgers. 2008. Molecular composition of the peri-islet basement membrane in NOD mice: a barrier against destructive insulitis. *Diabetologia* 51: 1680–1688.
31. Bentrem, D., and RJoehl, . 2003. Pancreas: healing response in critical illness. *Crit. Care Med.* 31: S582–S589.
32. Carlsson, P. O., S. Sandler, and L. Jansson. 1998. Pancreatic islet blood perfusion in the nonobese diabetic mouse: diabetes-prone female mice exhibit a higher blood flow compared with male mice in the prediabetic phase. *Endocrinology* 139: 3534–3541.
33. Fu, W., G. Wojtkiewicz, R. Weissleder, C. Benoist, and D. Mathis. 2012. Early window of diabetes determinism in NOD mice, dependent on the complement receptor CRIg, identified by noninvasive imaging. *Nat. Immunol.* 13: 361–368.
34. Huang, J. H., L. I. Cárdenas-Navia, C. C. Caldwell, T. J. Plumb, C. G. Radu, P. N. Rocha, T. Wilder, J. S. Bromberg, B. N. Cronstein, M. Sitkovsky, et al. 2007. Requirements for T lymphocyte migration in explanted lymph nodes. *J. Immunol.* 178: 7747–7755.
35. Dallas-Pedretti, A., M. McDuffie, and K. Haskins. 1995. A diabetes-associated T-cell autoantigen maps to a telomeric locus on mouse chromosome 6. *Proc. Natl. Acad. Sci. USA* 92: 1386–1390.
36. Calderon, B., J. A. Carrero, M. J. Miller, and E. R. Unanue. 2011. Entry of diabetogenic T cells into islets induces changes that lead to amplification of the cellular response. *Proc. Natl. Acad. Sci. USA* 108: 1567–1572.
37. Graham, K. L., B. Krishnamurthy, S. Fynch, R. Ayala-Perez, R. M. Slattery, P. Santamaria, H. E. Thomas, and T. W. H. Kay. 2012. Intra-islet proliferation of cytotoxic T lymphocytes contributes to insulitis progression. *Eur. J. Immunol.* 42: 1717–1722.